



Trans. Nonferrous Met. Soc. China 35(2025) 525-537

Transactions of Nonferrous Metals Society of China

www.tnmsc.cn



Effect of Cr₂O₃/Cr₃C₂ additions on mechanical and tribological properties of Ti(C,N)-based cermets

Mei-ling LIU^{1,2}, Ya-jing CAO¹, Wan-xiu HAI^{1,2}, Yu-hong CHEN^{1,2}

- 1. School of Materials Science and Engineering, North Minzu University, Yinchuan 750021, China;
- 2. Key Laboratory of Powder Material and Advanced Ceramics, North Minzu University, Yinchuan 750021, China

Received 10 January 2024; accepted 20 September 2024

Abstract: Cr₂O₃ was used as grain inhibitor in Ti(C,N)-based cermets with vacuum sintering. The microstructure and mechanical and tribological properties of cermets with Cr₂O₃ and Cr₃C₂ were investigated. The results show that adding Cr₂O₃ promotes a gray core/gray rim structure formation and finer size of Ti(C,N) hard phase. Compared with the cermet with an equal Cr₃C₂ addition, the cermet with 0.6 wt.% Cr₂O₃ exhibits 16.5% higher transverse rupture strength. This enhancement is likely due to the smaller lattice misfit at the core/rim interface and more uniform Cr distribution in the binder. Additionally, at room temperature (25 °C) and 800 °C, Cr₂O₃-containing cermets demonstrate lower coefficients of friction and volume wear ratios than Cr₃C₂-containing cermets, with the wear ratio difference reaching an order of magnitude. Scanning electron microscopy and X-ray photoelectron spectroscopy results further confirm more oxidation wear in Cr₂O₃-containing cermets than in Cr₃C₂-containing cermets.

Key words: Ti(C,N); Cr₂O₃; grain inhibitor; mechanical properties; tribological properties

1 Introduction

Owing to their low density, exceptional hightemperature oxidation resistance, remarkable wear resistance, and excellent hardness, Ti(C,N)-based cermets have been developed potential as alternatives to cemented carbide for furnishings and tooling applications [1-3]. These cermets consist of Ti(C,N) hard phase, metal binder phase, and carbides as their basic components. Typically, they exhibit a core-rim structure, with the Ti(C,N) hard phase constituting the core. To overcome the limited wettability between Ti(C,N) and the metal binder, various transition metal carbides have been utilized to improve mechanical performance of Ti(C,N)-based cermets, especially in terms of strength and toughness.

The sintering process of Ti(C,N)-based

cermets adheres to the Ostwald ripening rule, resulting in the formation of a rim composed of (Ti,M)(C,N) solid solution. During sintering, carbides dissolve and then re-precipitate to create this rim, and the use of different carbides leads to distinct enhancements in performance. For instance, QU et al [4] reported an exceptional 104% increase in the transverse rupture strength (TRS) with 25 wt.% WC additive in Ti(C,N)-Mo-Ni, which was attributed to solid solution strengthening and increased relative density. ZHENG et al [5] prepared Ti(C,N)-WC-Mo₂C-TaC-(Ni,Co) cermets with WC content variations ranging from 5.77 to 19.68 wt.%, obtaining the highest hardness and lowest wear ratio when the WC content was 19.68 wt.% at both 25 °C and elevated temperatures. ZHANG et al [6] examined the influence of WC content on the mechanical properties of Ti(C,N) cermets fabricated using TiO2, and the variations in

TRS, hardness, and $K_{\rm IC}$ followed a trend corresponding to the variation in WC content, reaching a peak value at 8 wt.%. LIU et al [7] reported that cermets with 5 wt.% Mo₂C and 5 wt.% TaC addition exhibited excellent hardness and fracture toughness values, reaching HRA 91.4 and $K_{\rm IC}$ of 13.5 MPa·m^{1/2}, respectively. QIU et al [8] found that Mo₂C addition inhibited the growth of ceramic particles and improved the tribological performance. GOU et al [9] added NbC to CoCrFeNi-bonded Ti(C,N) cermet, mechanical performance and wear resistance of the cermet were both enhanced. XU et al [10] explored the impact of TaC on the mechanical performance of Ti(C,N) cermet prepared via carbothermal reduction. LIN et al [11] demonstrated that VC addition could promote densification and enhance the mechanical properties and wear resistance. XIONG et al [12] confirmed that VC could decrease the lattice parameter of the rim phase and misfit of the core-rim structure, thus enhancing the mechanical performance. ZHANG et al [13] attempted to use VC and Cr₃C₂ together in Ti(C,N) cermets fabricated via carbothermal reduction, and all the cermets showed finer crystal size, while the cermet with Cr₃C₂ exhibited better mechanical properties. Cr₃C₂ has also been added to improve the hardness, TRS, and corrosion behavior of Ti(C,N) cermets [14–16]. Moreover, Cr₃C₂ has been shown to improve the high-temperature antioxidation performance as NiCr alloy [17,18].

As demonstrated earlier, previous studies have utilized VC and Cr_3C_2 as inhibitors to restrict grain growth, thereby reducing the crystal size of cermets and further enhancing their mechanical performance. Notably, VC and Cr_3C_2 have

traditionally been directly added to the cermet. However, to the best of our knowledge, there have been less reports of utilizing an inhibitor in the form of an oxide that is in-situ reduced to carbide for improving the performance of cermets. In this study, we introduced Cr_2O_3 to Ti(C,N) cermet in a one-step preparation via in-situ conversion to Cr_3C_2 and cermet sintering. In addition, a comparable content of Cr_3C_2 was added to create a reference sample. The objective was to investigate the impact of Cr_2O_3 as a new inhibitor on the microstructure and mechanical and tribological properties of Ti(C,N)-based cermets.

2 Experimental

2.1 Cermet preparation

The compositions of the cermets prepared using commercial raw powders are detailed in Table 1. For the $Ti(C_{0.7},N_{0.3})$ -WC-Mo₂C-Ni- $Cr_3C_2(x)$ cermets, 0, 0.5, 1, 1.5, and 2 wt.% of Cr_3C_2 were added, denoted as C0, C1, C2, C3, and C4, respectively. For the Ti(C_{0.7},N_{0.3})-WC-Mo₂C-Ni- $Cr_2O_3(x)$ -C cermets, 0.6, 1.3, 1.9 and 2.5 wt.% of Cr₂O₃ were added, denoted as CO₁, CO₂, CO₃, and CO4, respectively. Furthermore, the mass fraction of Cr₃C₂ produced by the carbothermal reduction of Cr₂O₃ in the COx cermets was equal to that of Cr₃C₂ in the Cx cermets. The process involved weighing the raw powders, mixing them, and subjecting them to wet-milling in a planetary ball mill at 400 r/min for 10 h. Subsequently, the mixtures were dried, sieved, and then pressed into green compacts under a pressure of 100 MPa. Finally, all the green compacts were sintered at 1450 °C under vacuum conditions.

Table 1 Chemical compositions of experimental cermets (wt.%)

Cermet	2 μm Ti(C,N)	3 μm WC	3 μm Mo ₂ C	6 μm Ni	3 μm Cr ₃ C ₂	3 μm Cr ₂ O ₃	100 nm C
C0	55	20	10	15	0		
C1	54.5	20	10	15	0.5		
C2	54	20	10	15	1		
C3	53.5	20	10	15	1.5		
C4	53	20	10	15	2		
CO1	54.4	20	10	15		0.6	0.21
CO2	53.7	20	10	15		1.3	0.44
CO3	53.1	20	10	15		1.9	0.65
CO4	52.5	20	10	15		2.5	0.85

2.2 Characterization

The phase structures of the sintered cermets were analyzed using X-ray diffraction with Cu K_a radiation (XRD-6000, Shimadzu, Japan). Scanning electron microscopy (SEM, SIGMA 500, Zeiss, Germany) was employed to observe the microstructure and morphology in backscatter (BSE) mode, and the distribution of elements in the cermets was assessed using energy-dispersive spectroscopy (EDS). Furthermore, transmission electron microscopy (TEM, Tecnai G2 F20, FEI, USA) was utilized to provide further confirmation of the microstructure. The transverse rupture strength (TRS) was determined using a three-point bending method conducted with a universal material testing machine according to ISO standard 3327:2009. The dimensions of the TRS samples were $20 \text{ mm} \times 3 \text{ mm} \times 4 \text{ mm}$, and the span was 16 mm. Vickers hardness measurements were carried out in accordance with the GB/T 37900-2019 standard, using a Wolpert-432SVD hardness tester with a 30 kg load applied for 15 s. The fracture toughness $(K_{\rm IC})$ was subsequently calculated as follows [19]:

$$K_{\rm IC} = 0.15 \sqrt{\frac{{\rm Hv}_{30}}{\sum_{i=1}^{4} L_i}}$$
 (1)

where Hv_{30} is the Vickers hardness (MPa), and L_i is the crack length (mm) in the optical microscope image.

2.3 Friction and wear testing

Friction and wear tests of the cermets were carried out by sliding them against a WC-6Co ball on a ball-on-disk friction test machine, both at room temperature (25 °C) and 800 °C. The applied load and rotation speed were set at 40 N and 1000 r/min, respectively. To examine the friction surface morphology of the cermets, a 3D surface profiler (Micro XAM) and SEM were utilized. The composition of the worn surfaces was determined through X-ray photoelectron spectroscopy (XPS, ESCALAB 250Xi, Thermo Fisher). Additionally, the wear volume (V) of the cermets was quantified using the 3D surface profiler. The wear rate (W_R) was calculated as the ratio of V to the product of the sliding distance (L) and normal load (F), as expressed in Eq. (2) [20]:

$$W_{\rm R} = V/(FL) \tag{2}$$

3 Results and discussion

3.1 Phase composition

In Fig. 1, the XRD patterns of cermets with varying Cr₃C₂ and Cr₂O₃ content are presented. The phase compositions of C1 and C0 are remarkably similar, with limited WC and Mo₂C forming a solid solution. Notably, the solid solution process of WC and Mo₂C is promoted with increasing Cr₃C₂ addition amount. When the mass fraction of Cr₃C₂ reaches 2% in the C4 cermet, the predominant phases consist of (Ti, W, Mo, Cr)(C, N) and Ni, with no detectable presence of WC and Mo₂C. Because the atomic radius of W and Mo is close to that of Ti, the peaks of (Ti,W,Mo,Cr)(C,N) can be identified as belonging to Ti(C,N), with PDF card number 42-1489. For comparison, C0 cermet is included. On the other hand, with increasing Cr₂O₃ content, the degree of solid solution between WC and Mo₂C initially increases and then decreases. In the case of CO2 cermet, which has an equivalent Cr₃C₂ content

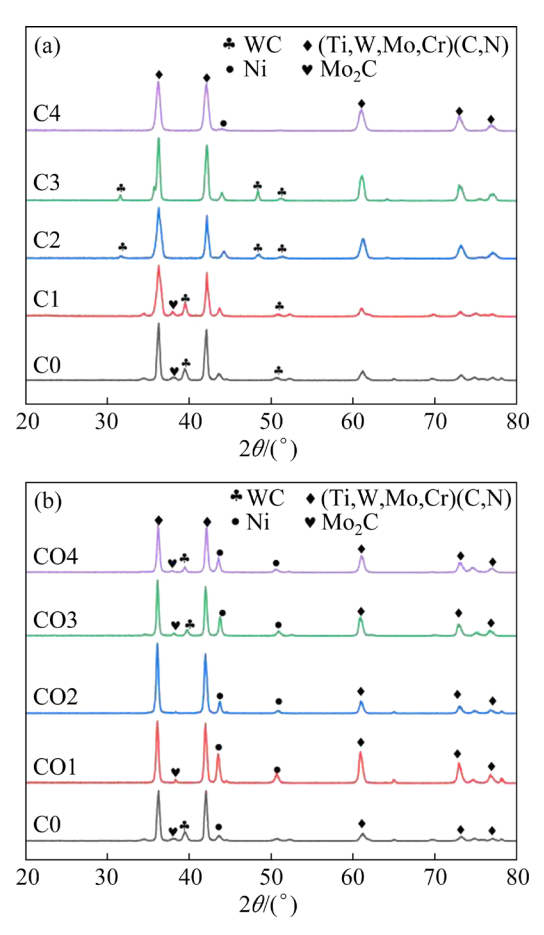


Fig. 1 XRD patterns of C0, C1, C2, C3, and C4 cermets (a); XRD patterns of C0, CO1, CO2, CO3, and CO4 cermets (b)

of 1 wt.%, the (Ti,W,Mo,Cr)(C,N) phase displays the highest peak intensity.

3.2 Morphology

Figure 2 shows the morphology and microstructure of C0, C1, C2, C3, and C4 cermets. In Fig. 2(a), the core—rim structure is not distinct, and bright pieces can be observed. According to BSE working mode, they are WC and Mo₂C, which are heavy elements. For the C1 cermet in Fig. 2(b), following the addition of 0.5 wt.% Cr₃C₂, bright pieces can still be observed, but the distribution of the gray rim around the black Ti(C,N) appears more homogeneous. As the amount of Cr₃C₂ increases, no bright pieces can be observed, aligning with the XRD patterns. The average grain size of Ti(C,N) in the C1 cermet is 0.91 μm, and it decreases to 0.86, 0.79, and 0.7 μm in C2, C3, and C4 cermets,

respectively. The Ti(C,N) grains become finer with increasing Cr₃C₂ content. The binder area of the C1 cermet was point-scanned using EDS, as shown in Fig. 2(c), revealing that Ti, Mo and W diffuse into the nickel binder.

Figure 3 shows the morphology and microstructure of the C0, CO1, CO2, CO3, and CO4 cermets. The Cr content in the CO1 cermet is equal to 0.5 wt.% Cr₃C₂, and the gray solid solution outside the gray rim appears to occupy a larger volume fraction, indicating that more Ti(C,N) grains participate in the solution reaction. Gray core/black rim structures can be observed, with light gray core/gray rim structures in the gray area. An EDS analysis of the light gray core and gray rim in Fig. 3(b) was conducted, as shown in Figs. 3(c, d). The results indicate that the composition of the light gray core is (Ti,W,Mo,Cr)C, and the fraction of W

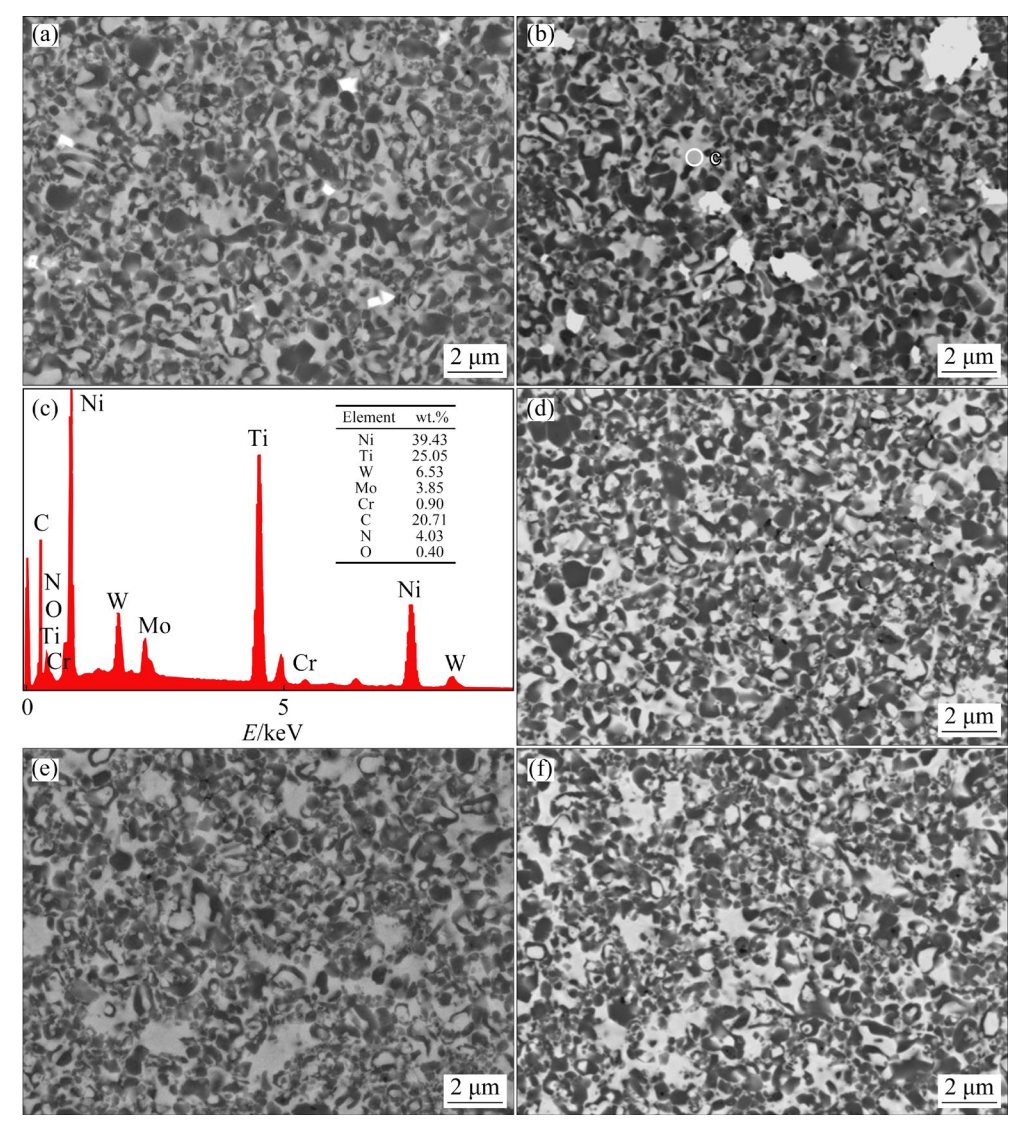


Fig. 2 SEM images of cermets: (a) C0; (b) C1; (c) EDS of selected binder area in (b); (d) C2; (e) C3; (f) C4

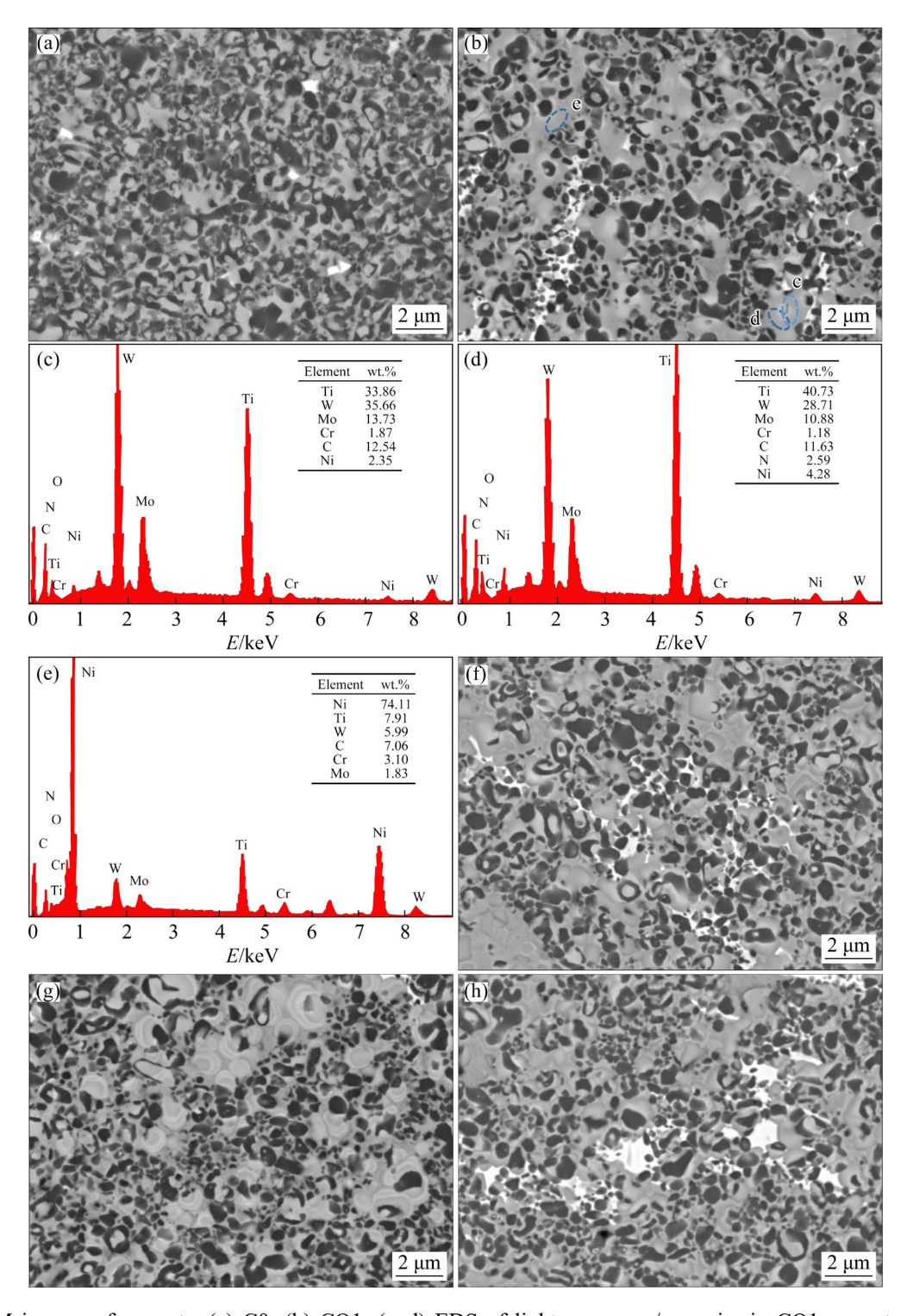


Fig. 3 SEM images of cermets: (a) C0; (b) CO1; (c, d) EDS of light gray core/gray rim in CO1 cermet; (e) EDS of selected binder area in (b); (f) CO2; (g) CO3; (h) CO4

element is relatively high. In contrast to the light gray core, the composition of the gray rim is (Ti,W,Mo,Cr)(C,N), and the Ti element content is high while the W element content is relatively low. EDS analysis was also used to examine the binder area in Fig. 3(b), as shown in Fig. 3(e). The results

confirm that the elements, including Ti, W, Mo, and Cr, diffuse into the nickel binder. In contrast to the C1 cermet, the Cr content is relatively high. This indicates that the Cr element originating from the Cr₂O₃ addition is distributed to a greater extent in the binder area, thus favoring the restriction of grain

growth and enhancing solid solution strengthening [21]. The average grain size of Ti(C,N) in the CO1 cermet is 0.8 µm, which indicates that the grain-refining effect of Cr₃C₂, reduced in situ by Cr₂O₃, is stronger than that of direct addition. The volume fraction of the gray solid solution was larger in the CO2 cermet, and the gray area starts to laminate. This lamination phenomenon is more evident in CO3 cermet, and the layer thickness increases. For the CO4 cermet, lamination becomes less distinct.

3.3 Microstructure

Figure 4 shows the high-angle annular dark-field (HADDF) and high-resolution transmission electron microscopy (HRTEM) images of the C1 and CO1 cermets. Combined with the results in Fig. 2(b), the typical black core/gray rim structure was selected as the observed area of the C1 cermet (Fig. 4(a)), and HRTEM was used to examine the interface, as shown in Fig. 4(b). The (111) plane of the Ti(C,N) core and (Ti,W,Mo,Cr)(C,N) rim exhibits a semi-coherent distribution at the phase interface. The interplanar spacing of Ti(C,N) is

0.248 nm, and the lattice parameter is 4.295 Å, while the interplanar spacing of (Ti,W,Mo,Cr)(C,N) is 0.233 nm, and the lattice parameter is 4.036 Å. The calculated lattice misfit is 6.03%. The light gray core/gray rim structure of the CO1 cermet is shown in Fig. 4(c), and HRTEM was used to examine the interface, as shown in Fig. 4(d). The (220) plane of the (Ti,W,Mo,Cr)C core and (Ti,W,Mo,Cr)(C,N) rim also exhibits a semicoherent distribution at the phase interface. The interplanar spacing of (Ti,W,Mo,Cr)C is 0.146 nm, and the lattice parameter is 4.130 Å, while the interplanar spacing of (Ti,W,Mo,Cr)(C,N) is 0.149 nm, and the lattice parameter is 4.214 Å. The calculated lattice misfit is 1.99%. A smaller lattice misfit results in less interface stress within the core-rim structure [22].

3.4 Mechanical properties

The mechanical properties of the COx and Cx cermets are shown in Fig. 5. As shown in Fig. 5(b), in contrast to C0, with the addition of Cr_3C_2 in the C1 to C4 cermets, the Vickers hardness increases, which can be attributed to the grain-refining effect

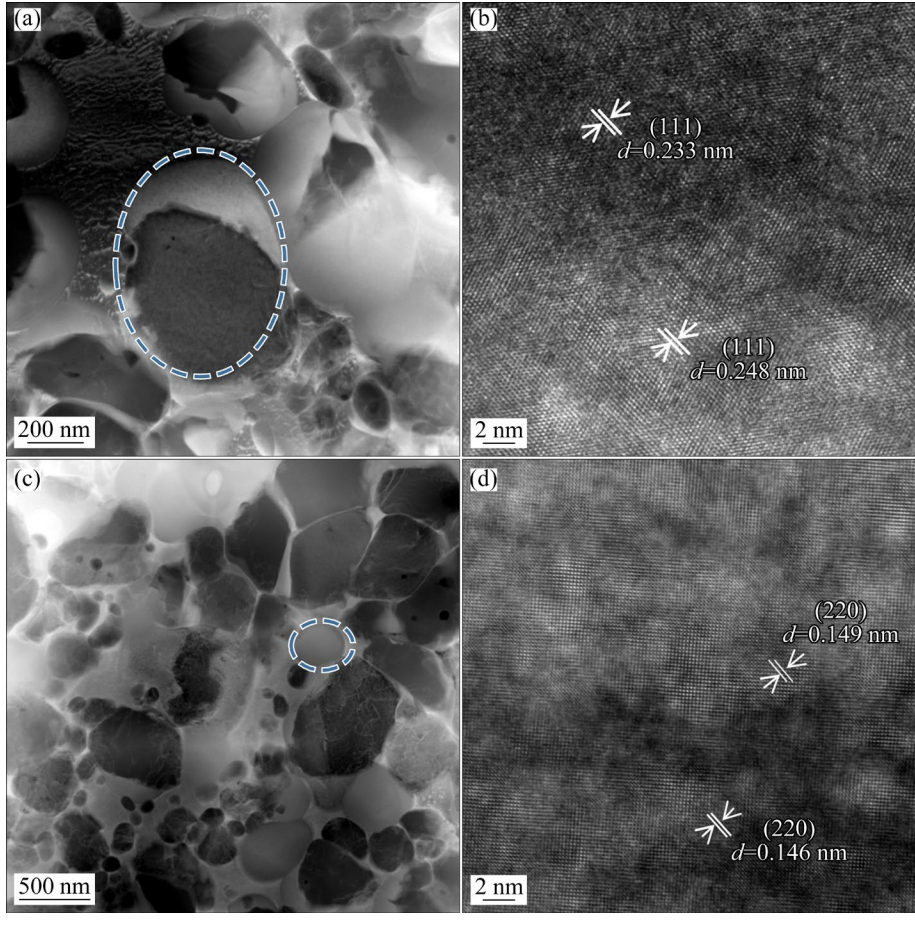


Fig. 4 HADDF (a, c) and HRTEM (b, d) images of C1 (a, b) and CO1 (c, d) cermets

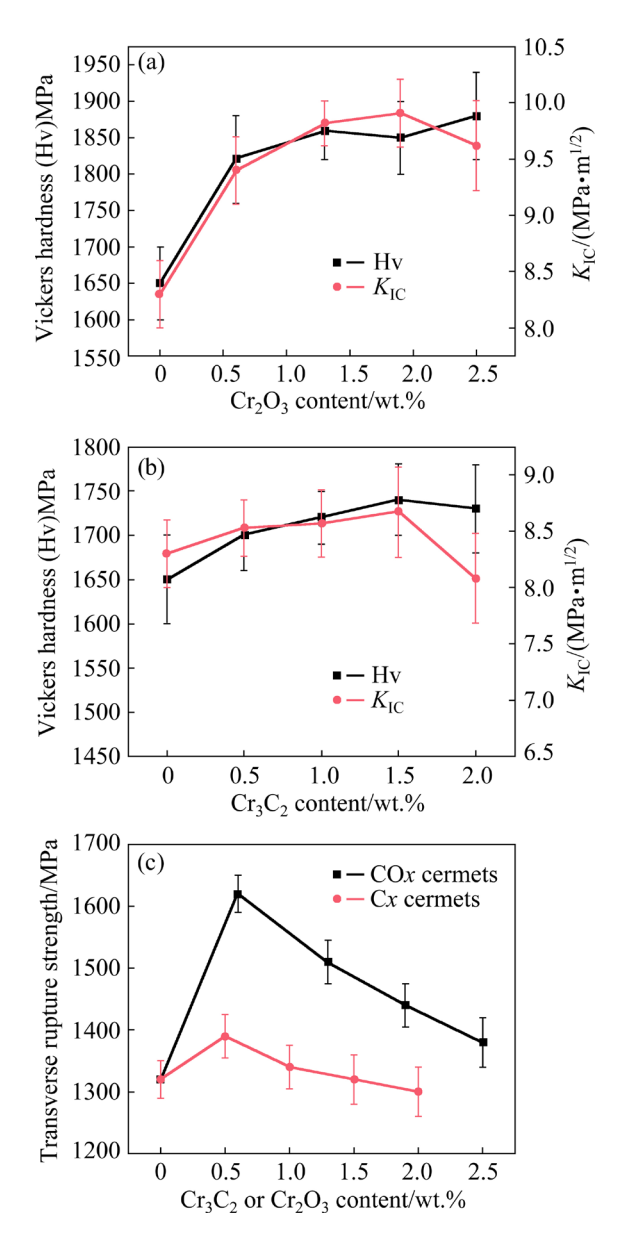


Fig. 5 Vickers hardness and fracture toughness of COx (a) and Cx (b) cermets; TRS of Cx and COx cermets (c)

brought by Cr₃C₂. Furthermore, the increase in fracture toughness can be ascribed to the more complicated core-rim structure formation, especially the gray core/black rim, as shown in Fig. 2. Figure 5(a) shows that the Vickers hardness and fracture toughness also increase with an increase in Cr₂O₃ content, because Cr₃C₂ obtained from the carbothermal reduction also participates in the solid solution reaction to refine the grains. Furthermore, Cr₂O₃-containg cermets exhibit a smaller grain size; consequently, the Vickers hardness of the COx cermets is higher than that of the Cx cermets. The average fracture toughness of the COx cermets is also higher than that of the Cx cermets because the COx cermets have more gray areas. Several laminations can be observed in the gray areas, especially in the CO2 and CO3 cermets. These laminations hinder crack extension and improve fracture toughness. The CO1 and C1 cermets, both with a Cr₃C₂ fraction of 0.5 wt.%, exhibit the maximum TRS values among the two types of cermets. The TRS values of the CO1 and C1 cermet are 1620 and 1390 MPa, respectively, with the former being 16.5% higher. From the EDS results shown in Figs. 2 and 3, the Cr is distributed to a greater extent in the binder area in the COx cermets. The alloying elements dissolving in the binder phase can hinder dislocation movements and enhance the rupture strength of materials. Therefore, the CO1 cermet exhibits enhanced mechanical performance, particularly in terms of TRS.

3.5 Friction and wear properties

The friction and wear tests of the C1 and CO1 cermets were conducted at room temperature (25 °C) and 800 °C. Figure 6(a) shows the COF variation curve for the C1 and CO1 cermets at room temperature and 800 °C. The average COFs of the C1 cermet at room temperature and 800 °C are 0.63 and 0.45, respectively. In contrast, the average COFs for the CO1 cermet are 0.47 and 0.35, respectively. These differences can be attributed to the high hardness of the CO1 cermet. For the CO1 cermet, the thermal COF is lower than the room temperature COF, which can be attributed to tribo-oxidation wear and adhesive wear [23,24]. Figures 6(b, c) show surface profiles of the cross-section of worn tracks after friction tests of the CO1 cermet at room temperature and 800 °C, respectively. Figures 6(d, e) show the surface profiles for the C1 cermet under the same conditions. The wear depth is in the order of ambient (room temperature) CO1 < thermal (800 °C) CO1 < ambient C1 < thermal C1. Figure 6(f) shows the volume wear ratio of the C1 and CO1 cermets. The room wear ratio of the C1 cermet is $8.55 \times 10^{-7} \,\mathrm{mm}^3 \cdot \mathrm{N}^{-1} \cdot \mathrm{m}^{-1}$, and the thermal wear ratio is $1.45 \times 10^{-6} \,\mathrm{mm^3 \cdot N^{-1} \cdot m^{-1}}$. The room wear ratio of the CO1 cermet is $1.7 \times 10^{-8} \, \text{mm}^3 \cdot \text{N}^{-1} \cdot \text{m}^{-1}$, and the thermal wear ratio is $5.65 \times 10^{-7} \text{ mm}^3 \cdot \text{N}^{-1} \cdot \text{m}^{-1}$. The room temperature and thermal wear ratios of the CO1 cermet are lower than those of the C1 cermet, which can be attributed to the higher hardness of the CO1 cermet [25].

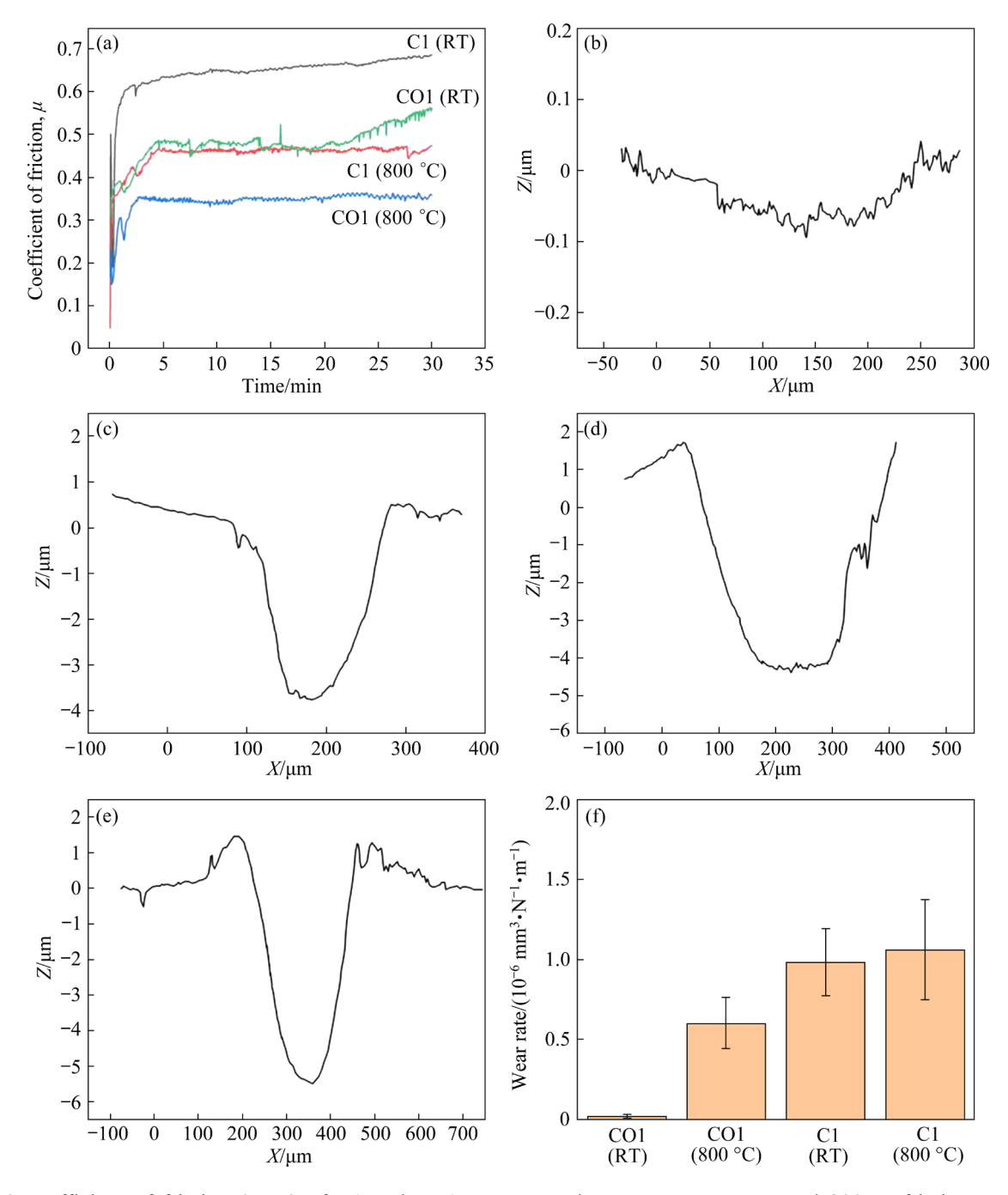


Fig. 6 Coefficient of friction (COF) of C1 and CO1 cermets under room temperature and 800 °C friction tests (a); Surface profiles of cross-section of worn tracks after friction tests of CO1 at room temperature (b), CO1 at 800 °C (c), C1 at room temperature (d), and C1 at 800 °C (e); Wear rates of C1 and CO1 cermet under room temperature and 800 °C friction tests (f)

The worn surface morphologies of the CO1 and C1 cermets after room temperature and 800 °C friction tests are shown in Fig. 7. No obvious friction traces can be observed on the worn surface of the CO1 cermet in Fig. 7(a). This is likely because little unreacted carbon remains, exhibiting a self-lubrication function. Figure 7(b) shows the 800 °C thermal worn surface of the CO1 cermet,

and a continuous oxidized tribolayer is present. Furthermore, the carbon that was not carbothermally reduced may have also lubricated the surface. In addition, the tribolayer could protect the worn surface, resulting in a lower COF and wear ratio [26]. The dominant mechanism of Cr₂O₃ cermets is tribo-oxidation wear. The worn surface morphology of the C1 cermet in Fig. 7(c) exhibits

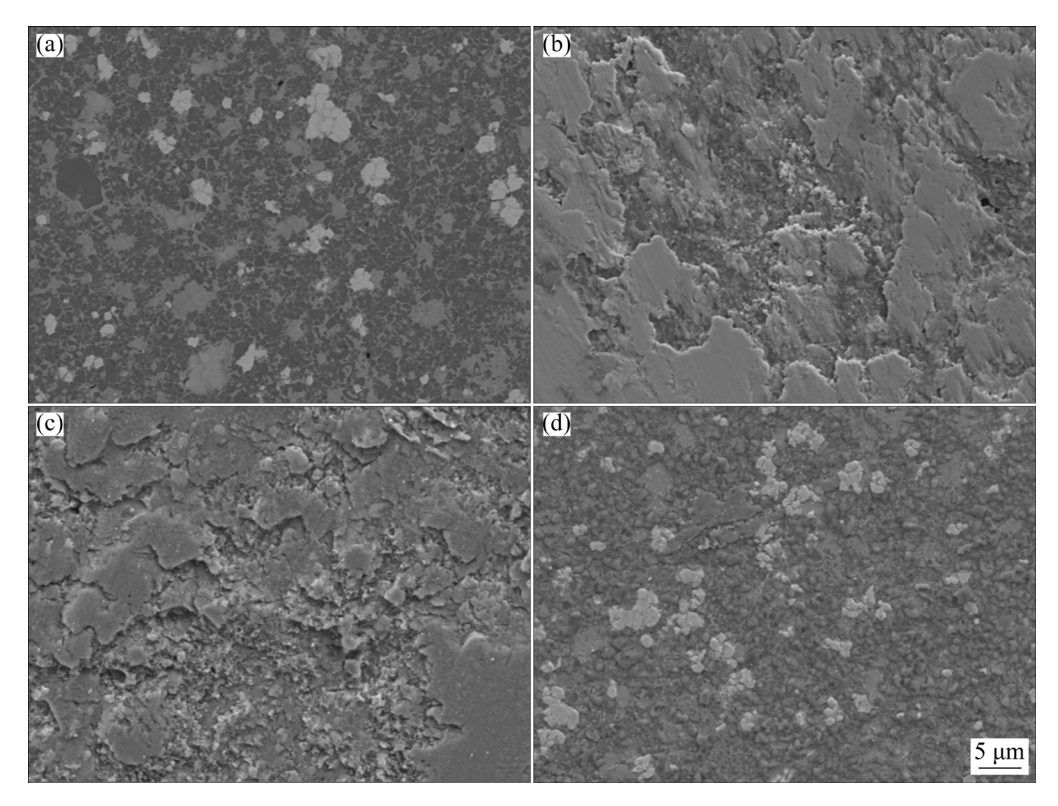


Fig. 7 Worn surface morphologies: (a) CO1 cermet after room temperature friction test; (b) CO1 cermet after 800 °C friction test; (c) C1 cermet after room temperature friction test; (d) C1 cermet after 800 °C friction test

adhesive wear, which explains the high room COF and wear ratio [27]. Figure 7(d) shows the worn surface of the C1 cermet after the thermal friction test, revealing some peeling traces. At 800 °C, the degree of metal binder softening becomes severe, and both adhesive wear and tribo-oxidation wear are pronounced. Combined with the high volume wear ratio of the C1 cermet, these results suggest that the tribo-oxidation layer is peeled by adhesive force, and the exposed surface exhibits welding points. The dominant mechanism of the cermets with Cr₃C₂ at 800 °C is adhesive wear. The roomtemperature worn surface morphology of the C1 cermet is similar to the thermal worn surface of the CO1 cermet, which is consistent with the volume wear ratio.

To analyze the species on the worn discs of the CO1 cermet, the chemical states of the elements were examined via XPS. The Ti 2p, Mo 3d, and W 4f spectra of CO1 after the room temperature abrasion test are shown in Figs. 8(a–c), and the corresponding spectra of CO1 after the 800 °C abrasion test are shown in Figs. 8(d–f). In Fig. 8(a), the peak at 455.4 eV corresponds to Ti 2p_{3/2} in Ti(C,N), while the peak at 464.5 eV corresponds to

Ti $2p_{1/2}$ in TiO₂ [28,29]. In Fig. 8(d), the peaks at 458.8 and 464.5 eV correspond to Ti 2p_{3/2} and Ti $2p_{1/2}$ in TiO₂, respectively. The results indicate that Ti(C,N) partially remains after the room temperature abrasion test, while the tribological product is primarily TiO₂ after the 800 °C test. In Fig. 8(b), the peaks at 228.9 and 232.2 eV can be attributed to Mo $3d_{5/2}$ in Mo₂C and Mo $3d_{5/2}$ in MoO₃, respectively [30]. In contrast, the peaks in Fig. 8(e) correspond to Mo $3d_{5/2}$ and Mo $3d_{3/2}$ in MoO₃. In Figs. 8(c, f), the peaks at 32.6 and 34.2 eV correspond to W $4f_{7/2}$ in WC and W $4f_{5/2}$ in WC, respectively. The peaks at 35.8 and 37.8 eV correspond to W $4f_{7/2}$ and W $4f_{5/2}$ in WO₃ [31]. Therefore, it can be inferred that WC and WO3 are present after the room temperature test while only the presence of WO₃ is detected after the 800 °C test for the CO1 cermet.

To examine the species on the worn disks of the C1 cermet, the chemical states of the elements were analyzed via XPS. The Ti 2p, Mo 3d, and W 4f spectra of C1 cermet after the room temperature abrasion test are shown in Figs. 9(a-c), and the corresponding spectra of C1 after the 800 °C abrasion test are shown in Figs. 9(d-f). In

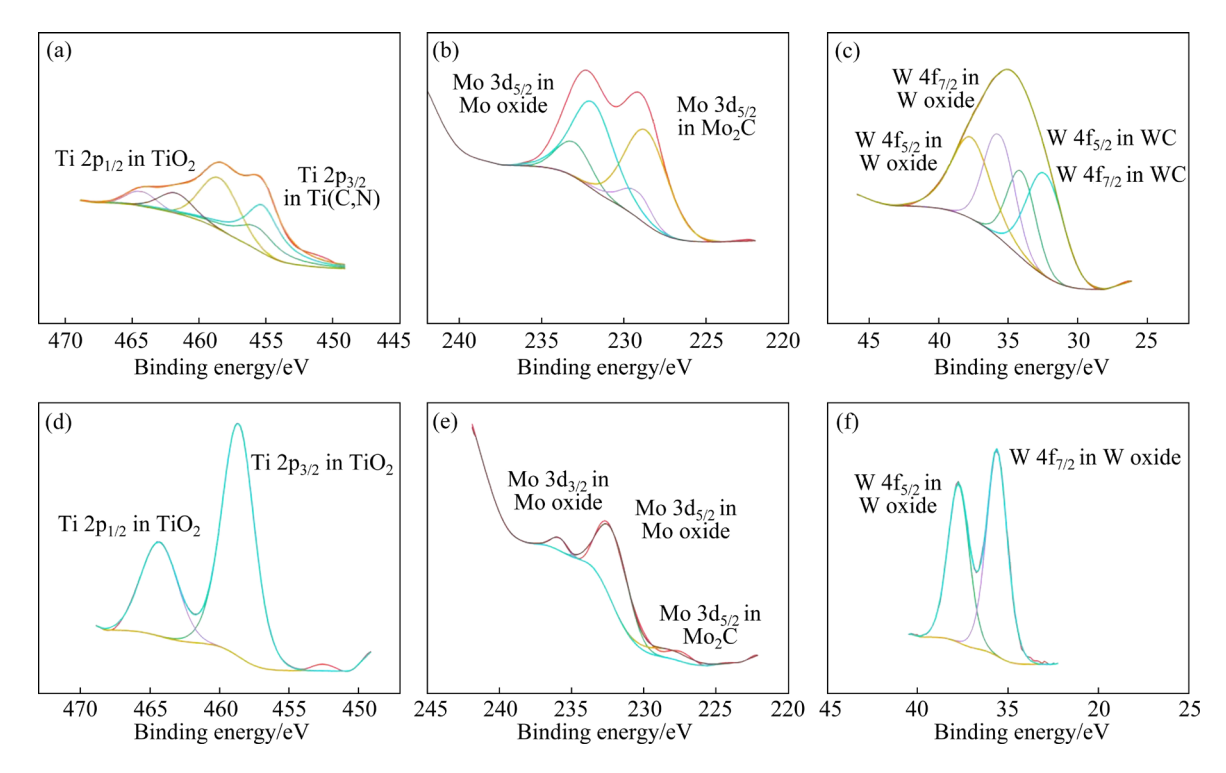


Fig. 8 XPS spectra of CO1 cermet after room temperature (a-c) and 800 °C (d-f) friction tests: (a, d) Ti 2p; (b, e) Mo 3d; (c, f) W 4f

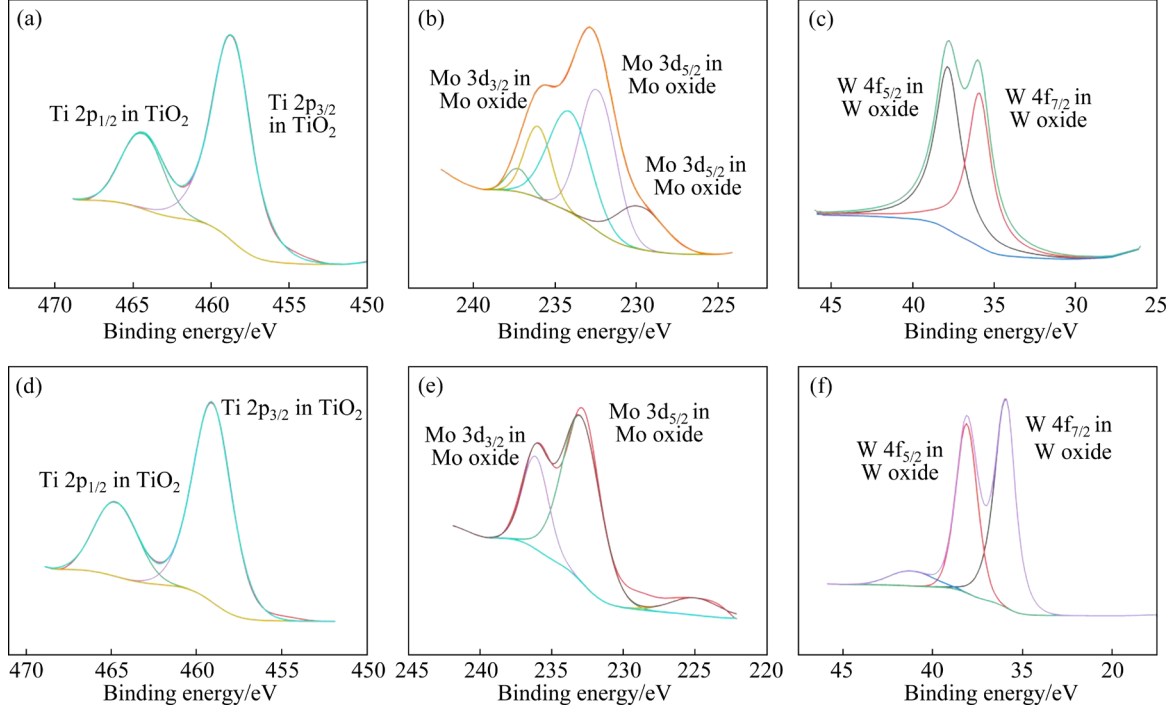


Fig. 9 XPS spectra of C1 cermet after room temperature (a-c) and 800 °C (d-f) friction tests: (a, d) Ti 2p; (b, e) Mo 3d; (c, f) W 4f

Figs. 9(a, d), both the peaks at 458.8 and 464.5 eV correspond to Ti $2p_{3/2}$ and Ti $2p_{1/2}$ in TiO₂, respectively. These results indicate that the Ti element in Ti(C,N) is oxidized to TiO₂ at room

temperature, exhibiting almost the same degree of oxidation as at 800 °C. Figure 9(b) shows that the oxidized products are mainly Mo oxides. However, some compounds with Mo are still present, which

can be attributed to (Ti,W,Mo,Cr)(C,N). Figure 9(e) indicates that the Mo element is almost completely changed to oxides. Figures 9(c, f) show that the compounds with W are nearly completely changed to oxides. The tribological surface of the C1 cermet is more oxidized than that of CO1 after the room temperature friction test. This is consistent with the smoother friction surface and minimum wear ratio of the CO1 cermet after the room temperature friction test.

4 Conclusions

- (1) The morphologies of Cr₂O₃-containing cermets show significant differences compared to those of Cr₃C₂-containing cermets. Notably, there is a higher volume fraction of solid solution in the Cr₂O₃ cermets, accompanied by the development of a gray core/gray rim structure. This particular morphology leads to a finer grain size in Ti(C,N) hard phase.
- (2) Cr₂O₃-containing cermets show enhanced Vickers hardness and TRS. This enhancement is primarily due to two factors: the greater Cr distribution within the binder region effectively limits grain growth and bolsters solid solution strengthening, and the smaller lattice misfit of the gray core/gray rim structure leads to less interface stress. Additionally, the fracture toughness benefits from the presence of the laminar solid solution.
- (3) At both ambient (25 °C) and elevated temperature (800 °C), the Cr₂O₃ cermets exhibit lower COF and volume wear ratios compared to the Cr₃C₂ cermets. The prevailing wear mechanisms in both cermet types are identified as tribo-oxidation wear and adhesive wear.

CRediT authorship contribution statement

Mei-ling LIU: Conceptualization, Methodology, Validation, Investigation, Writing — Original draft, Writing — Review & editing, Funding acquisition, Project administration; Ya-jing CAO: Data curation, Investigation, Validation; Wan-xiu HAI: Methodology, Resources; Yu-hong CHEN: Conceptualization, Formal analysis.

Declaration of competing interest

The authors declare that they have no known competing financial interests or personal relationships that could have appeared to influence the work reported in this paper.

Acknowledgments

This work was supported by the Natural Science Foundation of Ningxia, China (No. 2023AAC03284), the Fundamental Research Funds for the Central Universities Research Project of North Minzu University, China (No. 2022XYZCL04) and the Project of Key Laboratory of Powders and Advanced Ceramics, Co-founded by Ningxia and the State Ethnic Affairs Commission, China (No. 2103).

References

- [1] YUN Hao, ZOU Bin, WANG Jun. Effects of sintering temperature and nano Ti(C,N) on the microstructure and mechanical properties of Ti(C,N) cermets cutting tool materials with low Ni-Co [J]. Materials Science and Engineering A, 2017, 705: 98–104.
- [2] DONG Ding-qian, YANG Wei, XIANG Xin, HUANG Bo, XIONG Hui-wen, ZHANG Li, SHI Kai-hua. Microstructural evolution and phase transition mechanism of Ti(C,N)-based cermets during vacuum sintering process [J]. Ceramics International, 2021, 47(6): 8020–8029.
- [3] LENGAUER W, SCAGNETTO F. Ti(C,N)-based cermets: Critical review of achievements and recent developments [J]. Solid State Phenomena, 2018, 274: 53–100.
- [4] QU Jun, XIONG Wei-hao, YE Da-meng, YAO Zheng-hua, LIU Wen-jun, LIN Shao-jiang. Effect of WC content on the microstructure and mechanical properties of Ti(C_{0.5}N_{0.5})– WC-Mo-Ni cermets [J]. International Journal of Refractory Metals and Hard Materials, 2010, 28: 243–249.
- [5] ZHENG Zheng-hui, LV Jian, LOU Ming, XU Kai, CHEN Lei-lei, ZHANG Jian-bo, CHANG Ke-ke. Mechanical and tribological properties of WC incorporated Ti(C,N)-based cermets [J]. Ceramics International, 2022, 48: 10086–10095.
- [6] ZHANG Guo-tao, ZHENG Yong, KE Zheng, ZHANG Jia-jie, ZHAO Yi-jie, LU Xue-peng. Effect of WC content on the microstructure and mechanical properties of Ti(C,N)-based cermets fabricated by in situ carbothermal reduction of TiO₂ [J]. Materials Science and Engineering A, 2019, 761: 138024–138031.
- [7] LIU Chao, LIN Nan, HE Yue-hui. Influence of Mo₂C and TaC additions on the microstructure and mechanical properties of Ti(C,N)-based cermets [J]. Ceramics International, 2016, 42: 3569–3574.
- [8] QIU Hao, LI iao-qiang, PAN Cun-liang, FAN Jia-feng, QU Sheng-guan. Effect of Mo₂C addition on the formation of core-rim structure and mechanical properties of Ti(C,N)–WC-Mo₂C-(Ni,Co) cermet [J]. Journal of Materials Research and Technology, 2023, 25: 750-762.
- [9] GOU Qin-shan, XIONG Ji, GUO Zhi-xing, LIU Jun-bo, YANG-Lu, LI Xiang-rong. Influence of NbC additions on microstructure and wear resistance of Ti(C,N)-based cermets bonded by CoCrFeNi high-entropy alloy [J]. International

- Journal of Refractory Metals and Hard Materials, 2021, 94: 105375-105385.
- [10] XU Xiang-yu, ZHENG Yong, ZHAO Yi-jie, LU Xue-peng, KE Zheng, WU hao, YANG Min, LIANG Hai-feng. Influence of TaC content on microstructure and mechanical performance of Ti(C,N)-based cermets fabricated by mechanical activation and subsequent in situ carbothermal reduction [J]. Ceramics International, 2022, 48: 3826–3832.
- [11] LIN Nan, ZHAO Long-bo, ZOU Jia-cheng, MA Chao, WANG Zu-yong, HE Yue-hui. Improvement in densification process and properties of Ti(C,N)-based cermets with vanadium carbide addition [J]. Ceramics International, 2019, 45: 2692–2700.
- [12] XIONG Hui-wen, CHU Sheng-lin, LEI Peng-fei, LI Zhi-you, ZHOU Ke-chao. Ti(C,N)-based cermets containing uniformly dispersed ultrafine rimless grains: Effect of VC additions on the microstructure and mechanical properties [J]. Ceramics International, 2020, 46: 19904–19911.
- [13] ZHANG Guo-tao, ZHENG Yong, ZHANG Jia-jie, Ke Zheng, XU Xiang-yu, WU Hao, LU Xue-peng. Effect of VC/Cr₃C₂ additions on the microstructure, interface structure and mechanical properties of Ti(C,N)-based cermets prepared by in situ carbothermal reduction of nano TiO₂ [J]. Ceramics International, 2020, 46: 9698–9705.
- [14] WAN Wei-cai, XIONG Ji, GUO Zhi-xing, DONG Guangbiao, YI Cheng-hong. Effects of Cr₃C₂ addition on the erosion-corrosion resistance of Ti(C,N)-based cermets in alkaline conditions [J]. Tribology International, 2013, 64: 178–186.
- [15] WAN Wei-cai, XIONG Ji, YANG Mei, Guo Zhi-xing, DONG Guang-biao, YI Cheng-hong. Effects of Cr₃C₂ addition on the corrosion behavior of Ti(C,N)-based cermets [J]. International Journal of Refractory Metals and Hard Materials, 2012, 31: 179–186.
- [16] ZHAN Bin, LIU Ning, JIN Zhi-bo, LI Qi-long, SHI Jin-gang. Effect of VC/Cr₃C₂ on microstructure and mechanical properties of Ti(C,N)-based cermets [J]. Transactions of Nonferrous Metals Society of China, 2012, 22: 1096–1105.
- [17] ZHANG Mei-mei, LIN Nan, HE Yue-hui, KANG Xi-yue. A comparative study on microstructure and properties of Ti(C,N)-based cermets with the various Cr doping methods [J]. Journal of Alloys and Compounds, 2019, 799: 462–473.
- [18] ZHANG Mei-mei, JIANG Yao, LIN Nan, KANG Xi-yue, YAN Yan, HUANG Jian-hua, LIU Yi, QIU Song. Investigation of the oxidation behavior and high oxidationresistant mechanism of Ti(C,N)-based cermets [J]. Corrosion Science, 2020, 177: 108959–108971.
- [19] SCHUBERT W D, NEUMEISTER H, KINGER G, LUX B. Hardness to toughness relationship of fine-grained WC-Co hardmetals [J]. International Journal of Refractory Metals and Hard Materials, 1998, 16: 133-142.
- [20] MEDVEĎ D, BALKO J, SEDLÁK R, KOVALČÍKOVÁ A, SHEPA I, NAUGHTON-DUSZOVÁ A, BĄCZEK E, PODSIADŁO M, DUSZA J. Wear resistance of ZrB₂ based ceramic composites [J]. International Journal of Refractory

- Metals and Hard Materials, 2019, 81: 214-224.
- [21] ZHANG Mei-mei, HE Yue-hui, LIN Nan, KANG Xi-yue. Effects of carbon addition on the microstructure, mechanical properties, corrosion resistance and tribological behaviour of Ti(C,N)-based cermets [J]. Materials Research Express, 2018, 5: 126504–126520.
- [22] AHN S Y, KIM S W, KANG S. Microstructure of Ti(CN)—WC-NbC-Ni cermets [J]. Journal of the American Ceramic Society, 2004, 84: 843-849.
- [23] TIAN Yu-Xin, XIAO Hua-Qiang, YOU Chuan-chuan, FENG Jin-yu, XIAO Yi, ZHOU Xuan. High-temperature oxidation and wear properties of laser cladded Ti-Al-N composite coatings [J]. Transactions of Nonferrous Metals Society of China, 2023, 33: 1779–1791.
- [24] LI Zhan-jiang, FU Pei-xin, HONG Chun-fu, CHNAG Fa, DAI Pin-qiang. Tribological behavior of Ti(C,N)-TiB₂ composite cermets using FeCoCrNiAl high entropy alloys as binder over a wide range of temperatures [J]. Materials Today Communications, 2021, 26: 102095–102103.
- [25] LEYLAND A, MATTHEWS A. On the significance of the H/E ratio in wear control: A nanocomposite coating approach to optimized tribological behaviour [J]. Wear, 2000, 246: 1–11.
- [26] REN Ping, WEN Mao, ZHANG Kan, DU Su-xuan, ZHANG Yi-dan, CHEN Jian-hong, ZHENG Wei-tao. Self-assembly of TaC@Ta core-shell-like nanocomposite film via solid-state dewetting: Toward superior wear and corrosion resistance [J]. Acta Materialia, 2018, 160: 72–84.
- [27] CHEN Hao, WU Zi-hao, HAI Wan-xiu, LIU Li-meng, QIN Fa-lian, SUN Xiang-yun, LUO Tuo-sheng, SUN Wen-zhou. Microstructure, mechanical and tribological behaviour of TaC-SiC composites [J]. Journal of Ceramic Science and Technology, 2021, 12: 9–18.
- [28] LI Qi, XU Ji-liang, WANG San-mei, YU Kai-fu, ZHU Wen-kun, HOU Ting-ting, Lan-tian ZHANG, ZHANG Wen-hua, LIANG Shu-quan, WANG Liang-bing. Ti₃C₂T_xMXene doped by W atoms for full-spectrum photofixation of nitrogen [J]. Transactions of Nonferrous Metals Society of China, 2022, 32: 233–250.
- [29] XU Li-wei, LIN Nan, ZHAO Long-bo, MA Chao, WANG Zu-yong, HE Yue-hui. Effect of Ni contents on mechanical properties and corrosion behavior of Ti(C,N)–WC–Mo₂C– (Ni,Co) cermets [J]. Materials Chemistry and Physics, 2020, 252: 123253–123261.
- [30] KOU Zong-kui, WANG Ting-ting, PU Zong-hua, WU Lin, XI Kai, MU Shi-chun. Realizing the extraction of carbon from WC for in situ formation of W/WC heterostructures with efficient photoelectrochemical hydrogen evolution [J]. Nanoscale Horiz, 2019, 4: 196–201.
- [31] ZHOU Li-ming, XIONG Ji, GUO Zhi-xing, YE Jun-liu, LIU Jun-bo. Tribological performances of Ti(C,N)-based cermets with different graphite contents in dry sliding condition [J]. International Journal of Refractory Metals and Hard Materials, 2017, 68: 113–120.

加入 Cr₂O₃/Cr₃C₂ 对 Ti(C,N)基金属陶瓷力学和 摩擦性能的影响

刘美玲 1,2, 曹雅璟 1, 海万秀 1,2, 陈宇红 1,2

- 1. 北方民族大学 材料科学与工程学院,银川 750021;
- 2. 北方民族大学 粉体材料与特种陶瓷省部共建重点实验室, 银川 750021

摘 要:加入 Cr_2O_3 作为晶粒抑制剂,真空烧结制备 Ti(C,N)基金属陶瓷,研究陶瓷的显微组织、力学性能和摩擦磨损性能。结果表明: Cr_2O_3 促进灰芯/灰环结构的形成并减小 Ti(C,N)硬质相的粒径。和含等量 Cr_3C_2 的陶瓷对比,含 0.6%(质量分数) Cr_2O_3 陶瓷的抗弯强度提升 16.5%,这是由于灰色芯环结构界面处具有更小的晶格错配度和 Cr 元素在黏结剂中分布更加均匀。在 25 和 800 C摩擦磨损实验中,由于具有更高的硬度,含 Cr_2O_3 陶瓷具有更低的摩擦因数和磨损率,磨损率优于含 Cr_3C_2 陶瓷一个数量级。采用扫描电子显微镜和 X 射线光电子能谱进一步确认含 Cr_2O_3 陶瓷更多表现为氧化磨损。

关键词: Ti(C,N); Cr2O3; 晶粒抑制剂; 力学性能; 摩擦性能

(Edited by Bing YANG)